

# Directionally freeze-cast titanium foam with aligned, elongated pores

Yasumasa Chino <sup>a,\*</sup>, David C. Dunand <sup>b</sup>

<sup>a</sup> *Materials Research Institute for Sustainable Development, National Institute of Advanced Industrial Science and Technology, Nagoya 463-8560, Japan*

<sup>b</sup> *Department of Materials Science and Engineering, Northwestern University, Evanston, IL 60208, USA*

Received 10 August 2007; accepted 5 September 2007

Available online 23 October 2007

## Abstract

Directional freeze-casting – a process used to create foams with elongated, aligned pores applied so far exclusively for ceramics – is demonstrated for titanium foams. An aqueous slurry of <math><45\ \mu\text{m}</math> titanium powders was directionally solidified, resulting in a powder preform consisting of elongated, aligned dendrites of pure ice separated by interdendritic regions with high powder content. After freeze-drying to remove the ice dendrites and sintering to densify the powders, the resulting titanium foams exhibited 57–67% aligned pores ( $\sim 0.1$  mm wide and several millimeters long) replicating the ice dendrites. Because of the high powder oxygen content, the foams display high compressive strength and signs of embrittlement. Lower contamination was achieved by using purer  $<125\ \mu\text{m}</math> powders, but their larger size prevents the formation of pure ice dendrites (and thus elongated pores in the foam), in agreement with a model considering particle pushing and engulfment by a moving ice front.$

© 2007 Acta Materialia Inc. Published by Elsevier Ltd. All rights reserved.

**Keywords:** Foams; Porous material; Titanium; Powder processing; Freeze-casting

## 1. Introduction

Due to its low density, high strength and high chemical resistance, titanium is an attractive choice for the fabrication of foams for structural applications, e.g. as cores in sandwiches for structural applications [1,2], or for porous bone-replacement implants, where the excellent biocompatibility of titanium is essential [3–8]. Two main powder-metallurgy processes have been used to create titanium foams with high ( $>30\%$ ) porosity, as reviewed in Ref. [2], e.g. by powder sintering in the presence of a temporary space holder [9–11], or by creep expansion of entrapped argon [12–14]. However, very few reports describe titanium foams with aligned, elongated pores, which are of particular interest for filters, heat exchangers and biomedical implants. For the last of these applications, elongated pores mimic the

pore architecture of bone which is responsible for its structural and mechanical anisotropy [15].

One approach for creating aligned, elongated pores in titanium is to densify bundles of wires in the presence of argon, thus producing pressurized elongated pores which are then expanded by creep of the surrounding matrix [14]. The pressurized pore expansion method has also been used to produce elongated pores in preforms made of titanium powders, which are less expensive and more easily fabricated than titanium wires. In one case [12], equiaxed high-pressure pores were elongated and aligned by rolling or extruding the preform prior to their expansion. In another case [13], the pores were elongated during their expansion by application of a uniaxial stress. While the pores became aligned, their average aspect ratio was only  $\sim 2$ . Tuchinskiy and Loutfy [16] extruded rods, with a fugitive core and a shell made of titanium powder and polymer binder, which were cut in segments and compressed into a green body. The core material was removed at low temperature, forming elongated pores and the powders were vacuum-sintered at higher temperature. The authors suggested

\* Corresponding author. Tel.: +81 52 736 7461; fax: +81 52 736 7406.  
E-mail address: [y-chino@aist.go.jp](mailto:y-chino@aist.go.jp) (Y. Chino).

that aligned pores could be achieved by aligning the rod segments before pressing but did not address the issue of contamination by the core or binder materials.

Freeze-casting is an alternate, simple method to produce high aspect ratio pores in sinterable materials. While this process has been used to produce porous ceramics [17–23], it has never, to our knowledge, been applied to the creation of porous metals. In a first step, submicron ceramic powders are suspended in a liquid carrier which is usually water. Solidification of the slurry produces high aspect ratio dendrites of ice which reject and concentrate the powders into the interdendritic space. After complete solidification, the ice/powder composite is subjected to sublimation of the ice under vacuum, resulting in a powder preform with pores in the size and shape of the prior dendrites. Sintering of the preform leads to densification of the interdendritic ceramic powders into solid walls which surround the large pores, replicating the pure ice dendrites formed during freezing. Recently, using directional solidification of aqueous suspensions of submicron alumina powders, Deville et al. [22,23] demonstrated the formation of alumina foams with highly elongated, aligned pores. They showed that initial slurry composition and freezing conditions are important factors controlling the porous architecture of the foams.

The objective of the present investigation was to apply the freeze-casting method to the creation of titanium foams. As compared to the freeze casting of submicron alumina powders studied so far [19–23], the use of titanium powders raises additional issues. Titanium has 50% higher density than alumina and it is not available in the submicron powder sizes used for alumina, because of the extreme reactivity of titanium (and most metallic) powders in air when in the submicron range. Both the higher density and larger particle size result in a faster settling rate of the powder in water (thus making the use of thin slurries difficult) and a higher tendency for ice dendrites to engulf, rather than push, the powders. An additional issue for titanium powders, even when they are coarse enough to prevent pyrophoric reactions, is that their surfaces may be

oxidized by air during handling or by water during freeze-casting, thus increasing the oxygen content of the foams and leading to a steady reduction in tensile ductility up to an oxygen content of  $\sim 0.8$  wt.% where titanium becomes brittle in tension [24].

In this investigation, we explored for the first time the feasibility of using directional aqueous freeze casting to create titanium foams with elongated, aligned pores. Foams produced with two sizes of powders were tested mechanically in compression and the effects of oxygen contamination were investigated.

## 2. Experimental procedures

Unalloyed titanium powders with particle sizes  $<45 \mu\text{m}$  and  $<125 \mu\text{m}$  (called hereafter “fine” and “coarse”, respectively) were purchased from Aremco (Cottage, NY) and Starmet (Concord, MA), respectively. As shown in Fig. 1, the fine powders were irregular in shape (as is typical of the hydride–dehydride process), while the coarse powders were spherical (as is typical of the spraying process). A dry volume of  $\sim 2.8$  ml of powders (corresponding to a dry mass of 4.9 g of fine powders or 9.3 g of coarse powders) was added to  $\sim 3.5$  ml deionized water contained within a cylindrical glass vessel with 13 mm inner diameter and 38 mm height. The water had been de-aired under vacuum and contained 0.2 wt.% agar (Eden Foods, Clinton, MI) and a very small amount ( $\sim 1 \mu\text{l}$ ) of neutral detergent as surfactant. After stirring the powders to form a slurry, the vessel was placed on a copper chiller block held at 256 K in a freezer. The side of the vessel was insulated with polystyrene foam to minimize radial heat losses and thus maximize unidirectional freezing in the longitudinal, vertical direction. After release from the vessel, the frozen ice/titanium composite was sublimated for 24 h in a freeze dryer under a 7.5 Pa vacuum at 233 K. The resulting dried powder preform was pre-sintered under high vacuum of  $10^{-2}$  Pa at 573 K for 3 h and then sintered under  $10^{-3}$  Pa at 1423 K for 5 h for the fine powder preform and 1373 K

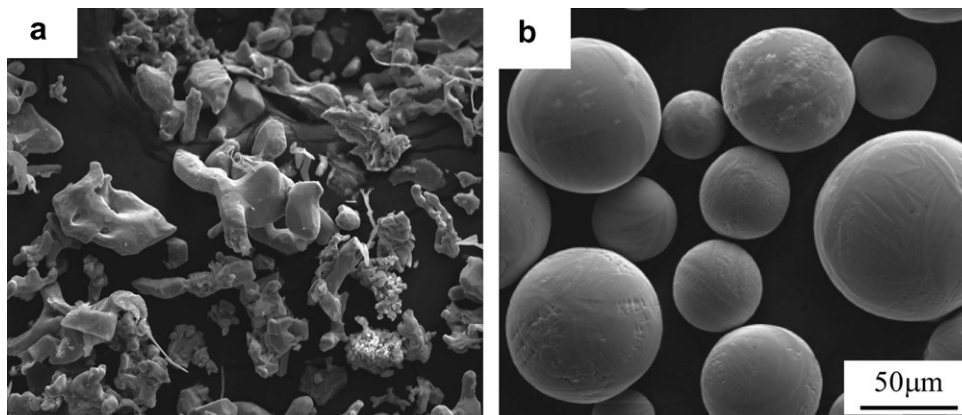


Fig. 1. SEM micrographs of Ti powders: (a) fine powders ( $<45 \mu\text{m}$ ), (b) coarse powders ( $<125 \mu\text{m}$ ).

for 2 h for the coarse powder preform. A fine powder control specimen was processed identically to the above procedures, except that the freezing and freeze-drying steps were not carried out. Instead, the water in the slurry, which was contained in a graphite vessel with 16 mm inner diameter and 40 mm height, was evaporated by holding at 356 K for 15 h. Finally, a dedicated sample was used to measure the ice front velocity during unidirectional freezing, using a fine alumina rod to determine the height of the frozen region at 15 min intervals.

The apparent density of the sintered samples was measured by the Archimedes method in deionized water, after coating with a thin layer of vacuum grease to prevent water penetration in open pores, thus yielding direct measurement of the total porosity. Also, the closed porosity was measured by helium pycnometry on selected specimens.

Metallographic examination was done by optical microscopy and scanning electron microscopy (SEM) on ground and polished samples whose porosity was filled with epoxy.

Uniaxial compression tests were carried out at room temperature with a constant crosshead displacement (with an initial strain rate of  $10^{-3} \text{ s}^{-1}$ ) on three electro-discharge-machined compression specimens with 4 mm diameter and 8 mm height. The first two specimens originated from the middle region of a foam with 60% porosity produced by freeze casting of fine powders and had their compression axis parallel or perpendicular to the ice freezing direction. The third specimen was machined from the top part of the control foam (with 60% porosity) produced by water evaporation of the fine-powder slurry, with its compression axis parallel to the vertical (powder settling) direction.

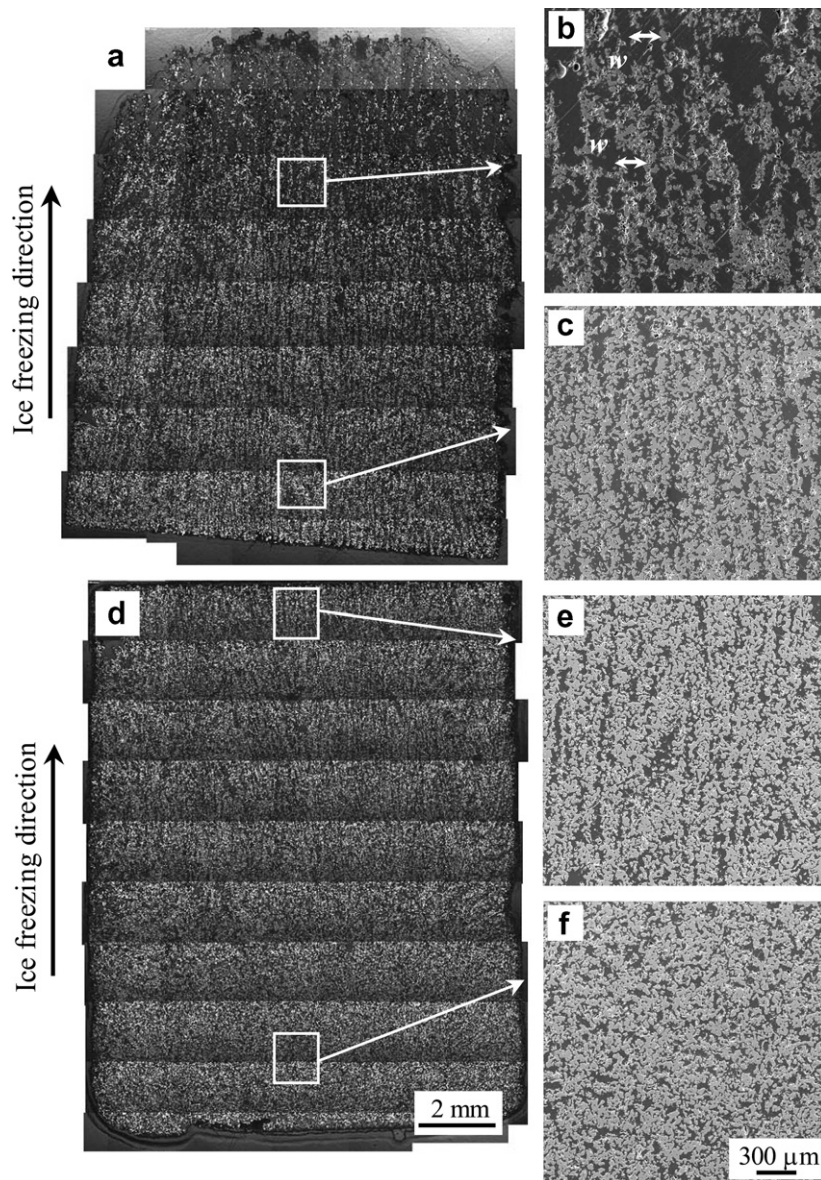


Fig. 2. Longitudinal section of foam produced by freeze casting of fine powder slurry. Optical micrograph montage for: (a) upper half (67% porosity); (d) lower half (57% porosity). Higher magnification SEM micrographs for: (b, c) regions highlighted in (a); (e, f) regions highlighted in (d). Elongated pores are more visible when viewing micrographs under a grazing angle. Solidification direction is vertical.

### 3. Results and discussion

#### 3.1. Foam produced by freeze casting of fine powders

Montages of optical micrographs showing a longitudinal cross-section of a foam freeze-cast with fine powders are shown in Fig. 2a for the upper half of the foam and in Fig. 2d for the lower half of the foam. Average total and closed porosities were 67% and 0.2% for the upper half and 57% and 0.2% for the lower half, respectively. At the base of the foam nearest to the chill, the pores were equiaxed (Fig. 2f). At a level  $\sim 10$  mm above the chilled bottom surface, high aspect ratio pores (with width of  $\sim 0.1$  mm and length of several millimeters) appeared and remained present up to the uppermost part of the foam. The pores visible in the longitudinal cross-section were aligned along the ice freezing direction and are separated by walls consisting of partially sintered titanium powders (Fig. 2b, c and e). As shown in Fig. 3a and b, a transverse cross-section (plane perpendicular to solidification direction) of the same foam shows mostly equiaxed pore cross-sections, confirming that the pores are well aligned in the solidification direction and illustrating that the walls are interconnected in the horizontal plane. A few elongated pores are visible in Fig. 3b and may be the result of dendrites growing radially. In the longitudinal sections, the average distance between walls – marked as  $w$  in Fig. 2b and corresponding to the structure wavelength as defined by Deville et al. [22,23] – was measured on micrographs shown in Fig. 2a and d and found to gradually increase from 150 to 180  $\mu\text{m}$  with increasing height above the specimen base, as shown by a best-fit line in Fig. 4. The error bars (corresponding to minimum and maximum values) increase near the top of the foam, probably because of powder depletion and slower ice growth rate.

The macrostructure of the control specimen produced by water evaporation without freezing is shown in Fig. 5a. Its average total and closed porosities were 60%

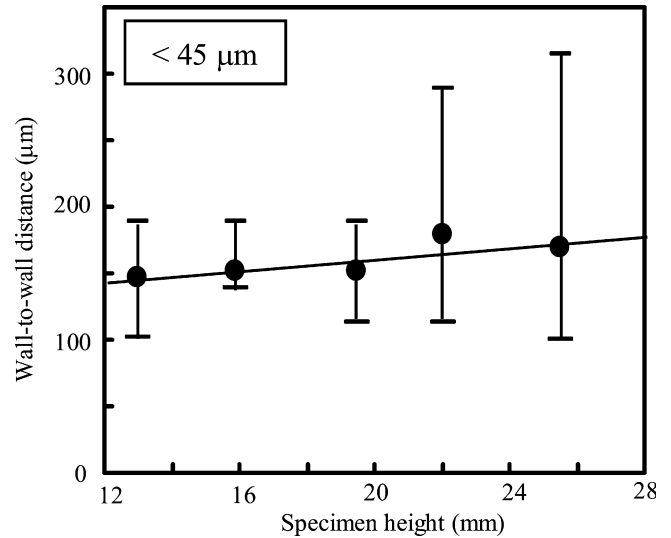


Fig. 4. Plot of wall-to-wall distance (illustrated in Fig. 2b) vs. specimen height for freeze-cast foam with fine powders.

and 0.6%, close to the values (62% and 0.2%) for the freeze-cast specimen shown in Fig. 2a–f, suggesting that the volume increase due to water freezing did not significantly affect the average foam porosity after sintering. However, the macrostructure of the control foam (Fig. 5a) was very different from that of the freeze-cast specimen (Fig. 2a and d): pores, equiaxed in shape and with a diameter  $\sim 50$   $\mu\text{m}$ , were present between the partially-sintered titanium powders (Fig. 5b), as expected from a partially-sintered preform of powders. Also, a small number of larger, near-spherical pores (170  $\mu\text{m}$  average diameter) were present in the control foam (Fig. 5b), and were probably caused by water vapor formation during evaporation. The equiaxed pore structure of the control foam produced by evaporation (Fig. 5a and b) confirms that the aligned walls observed in the freeze-cast foam (Fig. 2a–e) resulted from the growth of ice dendrites rejecting the powders in

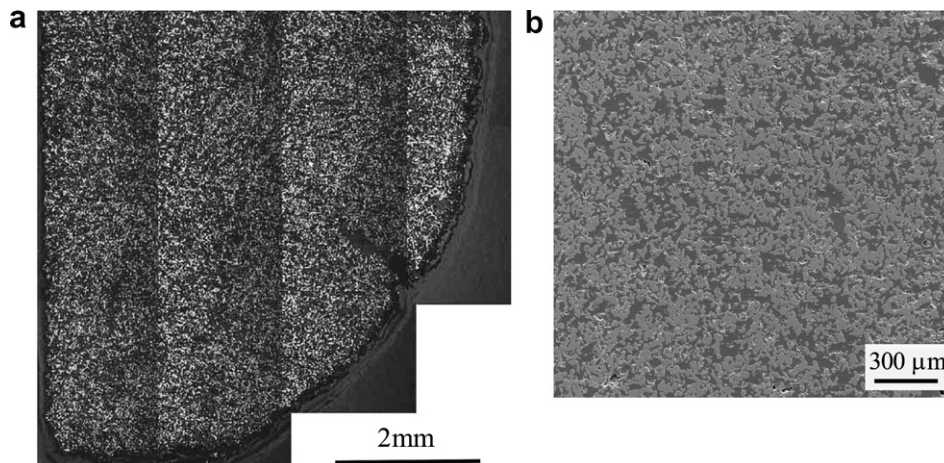


Fig. 3. Transverse section (plane perpendicular to solidification direction) for foam shown in Fig. 2, taken at a height midway between Fig. 2b and c. (a) Optical micrograph montage of quarter of foam (other quarters are similar). (b) Higher magnification SEM micrographs of transverse section.

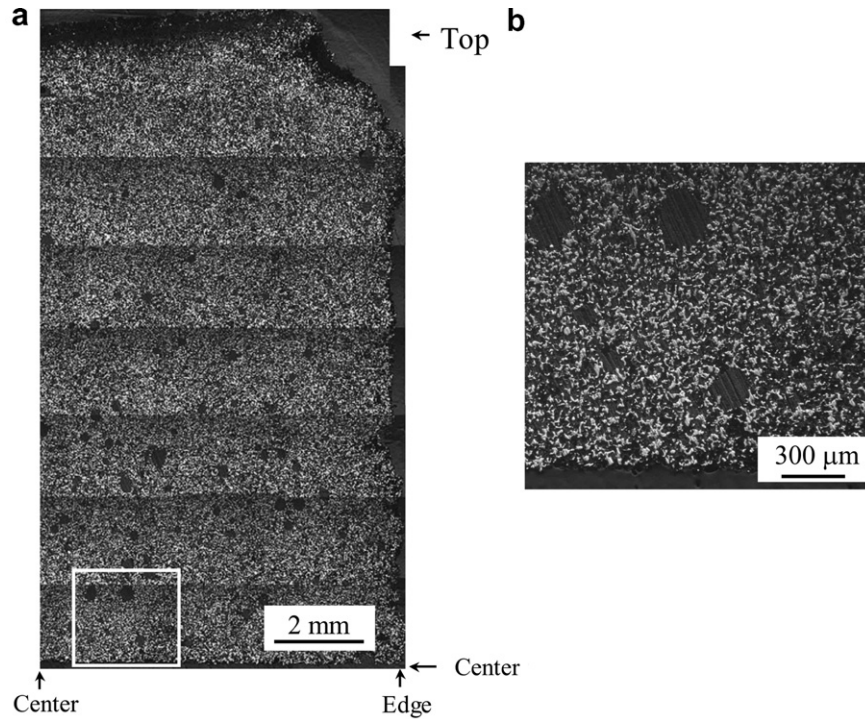


Fig. 5. Longitudinal section for control foam (60% porosity) produced by water evaporation of fine powder slurry: (a) optical micrograph montage of upper right quarter of foam (other quarters are similar), (b) higher magnification SEM micrographs of region highlighted in (a).

the interdendritic space, where they accumulated and subsequently sintered during heat-treatment. The equiaxed shape of the pores at the bottom part of the freeze-dried foam (Fig. 2f) most probably represents replication of equiaxed ice crystals, as also reported by Deville et al. in alumina foams [23]. These equiaxed pores near the base of the freeze-cast foam (Fig. 2f) had about twice the diameter (~8 times the volume) of those visible in the control unsolidified foam (Fig. 5b), indicating that powders were probably pushed by the growing equiaxed ice crystals.

Fig. 6 shows the variation in ice front velocity as a function of ice height for directionally freeze-cast specimens with fine and coarse powders. The ice front velocity was unaffected by the powder size, and exhibited a maximum value at a height of 12 mm, corresponding to the first data point in the dendritic zone. With increasing ice height, the ice front velocity decreased monotonously, as expected from the much lower thermal conductivity of ice as compared to copper. This decrease in ice velocity is consistent with the increase in wall-to-wall distance shown in Fig. 4. Indeed, Deville et al. [22,23] showed for freeze-cast alumina slurries that a decrease in ice front velocity leads to an increase in ice dendrite tip radius, due to a drop in supercooling ahead of the ice interface and thus an increase in the structure wavelength (alumina wall-to-wall distance). Miyawaki et al. [25,26], in an investigation of ice crystal size of pure water and aqueous agar solutions, also found that the ice dendrite size is inversely proportional to ice front velocity. Fig. 7 shows the best-fit line through the experimental data (ice front velocity vs. mean dendrite size) measured by Miyawaki et al. [27], together with the wall-

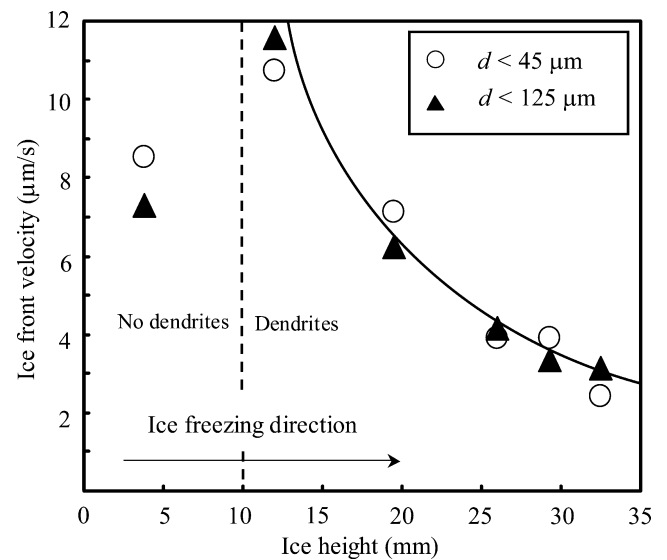


Fig. 6. Plot of ice front velocity vs. ice height for slurries of fine and coarse powders.

to-wall distance found in the present fine-powder foam. The good correlation between both sets of data is evidence that the ice dendrite formed by unidirectional freezing were replicated, most probably faithfully, into pores in the present sintered foams.

### 3.2. Foam produced by freeze casting of coarse powders

Fig. 8 shows a longitudinal section of the bottom half of the freeze-cast foam produced with coarse powders, with

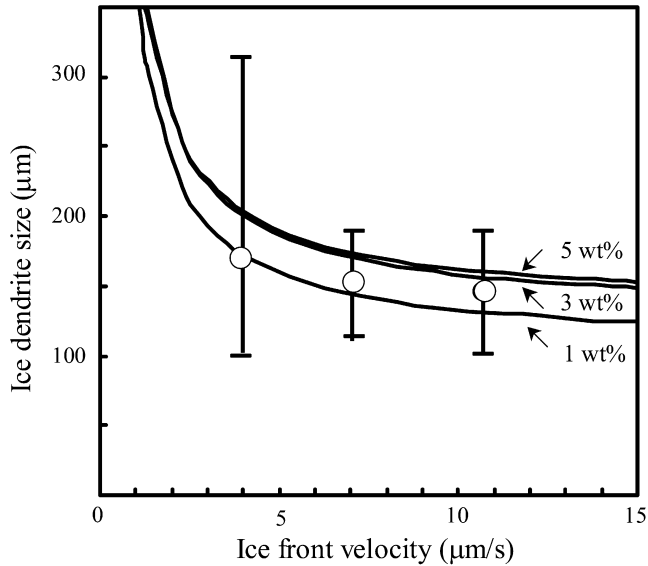


Fig. 7. Plot of wall-to-wall distance in fine-powder foams (with 0.2 wt.% agar) vs. ice front velocity. Best-fit lines for experimental data [27] of ice front velocity vs. mean ice dendrite size are also shown for various agar concentrations.

total and closed porosities of 38.1% and 1.3%. The upper half, with porosities of 38.9% and 0.8%, exhibited the same structure and is not shown. This foam did not exhibit elongated pores, despite having been freeze-cast under the same conditions and with the same ice front velocity as the fine-powder foam displaying elongated pores (Fig. 2a–e). The lack of clearly defined dendrites may be due to the similarity in the powder size and ice dendrites diameter. Another, more likely reason is that the large powders were entrapped by the growing dendrites, rather than being pushed into the

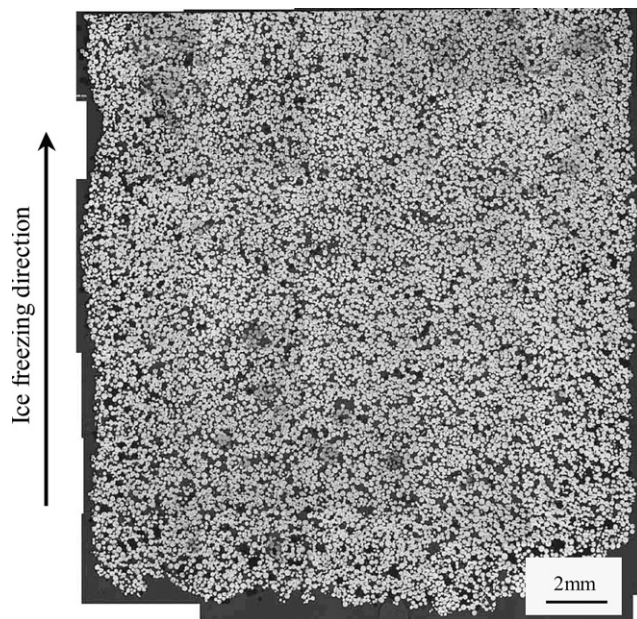


Fig. 8. Longitudinal section for bottom half of foam produced by freeze casting of coarse powder slurry (38% porosity) shown in optical micrograph montage.

interdendritic spaces. This hypothesis is discussed in the following.

Deville et al. [22,23] estimated a critical size above which suspended particles are trapped by the moving water–ice front. They used a force balance between viscous drag during particle pushing (favoring entrapment) and the repulsive molecular interaction at the particle/ice interface (favoring pushing). In our study, the effects of gravity and buoyancy forces were taken into consideration because of the much larger particle size as compared to the alumina particles used in Refs. [22,23]. Here, the critical ice front velocity was estimated using another simple theoretical model developed for the ideal case of smooth spherical particles interacting with a planar freezing front [28]. Under steady-state conditions, the force experienced by the particle is the sum of attractive forces (gravity and viscous drag forces), oriented downwards and favoring entrapment, and repulsive forces (buoyancy and molecular van der Waals forces), oriented upwards and favoring pushing. Setting to zero this sum of forces (for which expressions are given in Ref. [28]) and assuming that the particle and ice velocity are the same, provide the critical ice front velocity,  $v_c$ , above which particles are engulfed by the moving ice front and below which they are rejected from the ice front

$$v_c = \frac{\rho_l}{9\eta\rho_s} \left[ \frac{-A}{2\pi d\delta_0} - gd\delta_0(\rho_p - \rho_l) \right] \quad (1)$$

where  $d$  is the particle diameter,  $A$  is the Hamaker constant of the ice–water–particle system ( $A = -7.0 \times 10^{-20}$  J [29]), assuming that the oxidized particle surface is  $\text{TiO}_2$  [30],  $\eta$  is the viscosity of the liquid phase ( $\eta = 0.0018 \text{ m}^3 \text{ s}^{-1}$  [31] for water, assumed to be unaffected by the small agar solute content),  $\delta_0$  is the minimal distance between the particle and the freezing front ( $\delta_0 = 1 \text{ nm}$  [28,32]),  $\rho_p$  is the particle density ( $\rho_p = 4500 \text{ kg m}^{-3}$ ),  $\rho_s$  and  $\rho_l$  are the densities of the solid and liquid phase ( $\rho_s = 920 \text{ kg m}^{-3}$  for ice,  $\rho_l = 1000 \text{ kg m}^{-3}$  for water) and  $g$  is the gravitational constant.

The critical ice front velocity, as determined from Eq. (1), is plotted as a function of particle diameter in Fig. 9. Also shown are the experimental data for the two sizes of powders, based on the measured velocity range shown in Fig. 6. Despite significant uncertainties in some of the parameters (in particular the value of  $\delta_0$ ), the model correctly predicts that the fine powders ( $<45 \mu\text{m}$ ) are pushed by the growing dendrites and that the coarse powders ( $<125 \mu\text{m}$ ) are, for the most part, entrapped by the advancing ice front.

### 3.3. Foam oxygen content

One challenge associated with the aqueous freeze casting of titanium powders is the formation of a surface layer composed of oxide  $\text{TiO}_2$  and its hydrated oxide ( $\text{TiO}_2\text{H}_2\text{O}$ ) [33]. Table 1 lists oxygen and hydrogen concentrations of the as-received powders and the freeze-cast foams as measured by ATI Wah Chang (Albany OR)

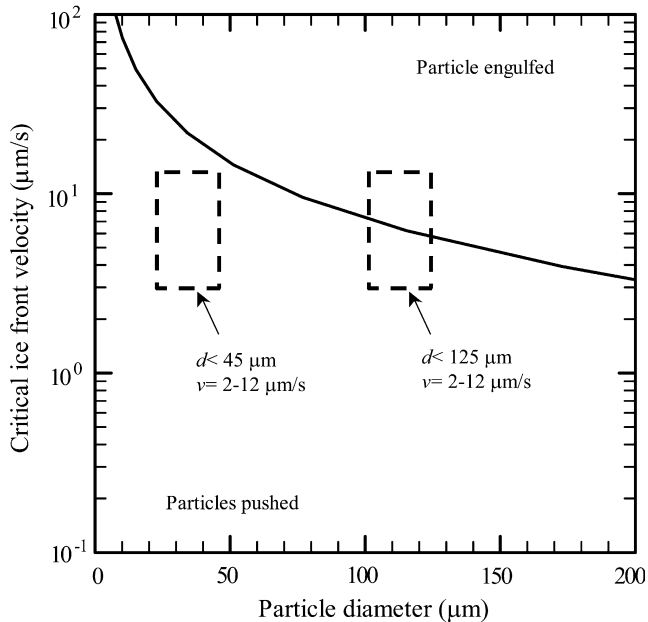


Fig. 9. Plot of critical ice front velocity vs. Ti particle size (Eq. (1)), above which particles are engulfed in the ice and below which particles are pushed by the ice dendrites.

using the combustion–infrared-emission method. As expected from the vacuum sintering step, the hydrogen concentration of both foams was below the level where severe embrittlement occurs in pure titanium [34]. Oxygen contents for the coarse powders (0.16 wt.%) and the corresponding freeze-cast foam (0.24 wt.%) were also below the embrittlement level. However, the oxygen content of the as-received fine powders (3.4 wt.%) was much higher than the critical value ( $\sim 0.8$  wt.%) above which tensile ductility of titanium becomes small [24]. After freeze casting, the oxygen content of the fine-powder foam increased by 0.4 wt.%, which is five times the gain observed for the foam made with coarse powders. This higher gain was expected in view of the larger specific area of the fine powders, due to both their smaller size and their less spherical shape (Fig. 1). However, the twentyfold increase in powder initial oxygen content from coarse to fine powders (from 0.16 to 3.4 wt.%) is unlikely to be due solely to the higher specific area and probably reflects different production histories.

The first effect of this high level of oxygen is a steep increase in the  $\alpha \rightarrow \alpha + \beta$  transus temperature. With 3.8 wt.% O, the transus is above the sintering temperature,

Table 1  
Oxygen and hydrogen concentration of as-received titanium powders and freeze-cast titanium foams

Material	Oxygen (wt.%)	Hydrogen (ppm)
Ti powder (<125 $\mu\text{m}$ )	0.16	26
Ti foam (<125 $\mu\text{m}$ )	0.24	180
Ti powder (<45 $\mu\text{m}$ )	3.4	1600
Ti foam (<45 $\mu\text{m}$ )	3.8	880

so that the fine-powder foams were sintered in the  $\alpha$ -Ti field. Since self-diffusion is slower for  $\alpha$ -Ti than for  $\beta$ -Ti [35], this reduces the extent of powder densification achieved during the sintering step. Given that titanium rapidly dissolves its oxides at elevated temperature [36], densification is, however, expected to be unhindered by the oxide layer present on the fine powders (an upper bound of whose thickness is calculated as 0.7  $\mu\text{m}$ , assuming a spherical shape for the fine powders).

A second expected effect of the elevated oxygen content of the fine-powder foams is a large increase in strength and concomitant decrease in tensile ductility, as measured in non-porous titanium [24]. As discussed in the following paragraph, the fine-powder foams indeed showed sign of oxygen-induced strengthening and embrittlement. One option to address this issue would be to increase the size of the powders to reduce oxygen contamination. Fig. 9 predicts that somewhat coarser titanium powders (i.e. in the range of 50–70  $\mu\text{m}$ ), which should have markedly lower oxygen contamination tendency than the present fine powders ( $<40$   $\mu\text{m}$ ), would allow the formation of dendrites for freezing velocities as high as  $\sim 10$   $\mu\text{m s}^{-1}$  (36  $\text{mm h}^{-1}$ ). Such powders may, however, be too coarse to produce a self-standing preform after ice removal and the resulting foams might display cell walls with a width nearly equal to the powder size, resulting in very irregular wall surfaces. It thus seems that a better strategy would be to use fine titanium powders (in the range 20–50  $\mu\text{m}$ ) with lower initial oxygen content than the present  $<45$   $\mu\text{m}$  powders. A future publication will report on foams produced with such powders.

### 3.4. Foam compressive properties

Fig. 10 shows the engineering compression stress–strain curves of three fine-powder foams: two unidirectionally freeze-cast foams (with their pores oriented parallel and perpendicular to the compression axis) and the control foam produced by water evaporation. The total porosity of the three specimens was 60%. The curves are characterized by an initial elastic region, a yield stress of 40–60 MPa, a sharp stress drop (for the two higher-strength foams) and a long plateau region with a nearly constant flow stress of  $\sim 15$  MPa, terminated by a densification region where the flow stress increases rapidly. This overall behavior is characteristic of ductile metallic foams [37]. However, the freeze-cast specimen with pores parallel to the applied stress was crushed after  $\sim 45\%$  strain without reaching the densification region and all curves exhibited serrations; both effects are indicative of embrittlement [38]. This is expected, given the very high oxygen content of the titanium, which is well beyond the value of  $\sim 1$  wt.% O resulting in near-zero tensile ductility in titanium. However, since pore walls deform primarily in compression and/or bending, some residual ductility under these deformation modes may have been retained even at these very high oxygen concentrations, resulting in the sizeable energy

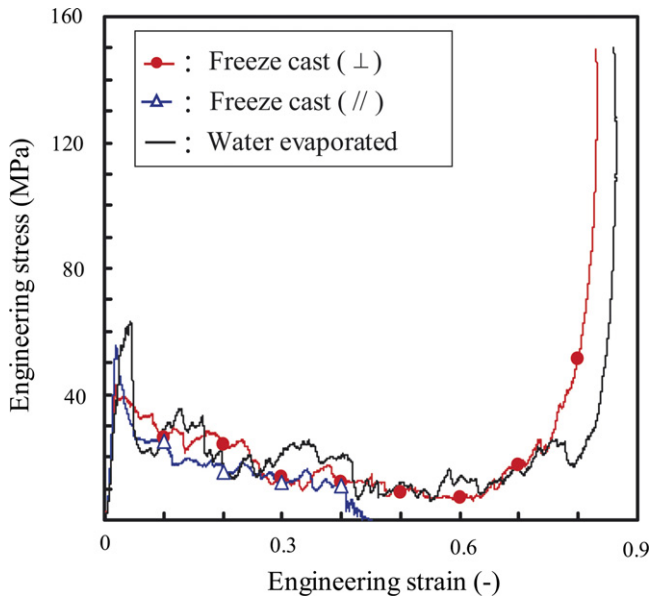


Fig. 10. Engineering compression stress–strain curves of foams processed by unidirectional freeze casting (two orientations of load with respect to freezing direction) and by water evaporation. All three specimens have the same 60% porosity.

absorption measured from the stress–strain curves ( $\sim 15 \text{ MJ m}^{-3}$  up to densification).

Here, we do not attempt to compare the yield stress of the freeze-cast foams to the widely used relationship for ductile metallic foams:

$$\frac{\sigma}{\sigma_{\text{sl}}} = 0.3 \left( \frac{\rho}{\rho_{\text{sl}}} \right)^{3/2} \quad (2)$$

where  $\sigma$  is the foam yield stress,  $\sigma_{\text{sl}}$  is the solid yield stress,  $\rho$  is the foam apparent density and  $\rho_{\text{sl}}$  is the solid density. This is because the compressive yield strength of titanium with 3.8 wt.% O is unknown (but expected to exceed a yield stress of 900 MPa for 0.75 wt.% O [24]) and because Eq. (2) is applicable only to foams with equiaxed pores. For comparison purpose, Eq. (2) can, however, be used to provide the yield stress of a hypothetical foam with 0.25 wt.% O (a typical value for coarse Ti powders and corresponding to  $\sigma_{\text{sl}} = 280 \text{ MPa}$  [34]) and a relative density of 0.40 (corresponding to the 60% porosity of the present freeze-cast foams). The resulting value of 21 MPa is significantly lower than measured for the freeze-cast foams (40–60 MPa; Fig. 10), indicating that strengthening due to the high oxygen concentration exceeds weakening from the notches present in the partially sintered walls, or the non-spherical shape of the pores.

#### 4. Conclusions

Titanium foams with aligned, elongated pores were created by directional freeze casting of titanium powders. In this process, an aqueous powder slurry is directionally solidified at rates sufficiently slow that pure ice dendrites form and reject the powders to interdendritic regions.

The ice dendrites are then removed by freeze drying, leaving pores that replicate their shape. Finally, sintering of the interdendritic powders results in continuous titanium walls separating the pores. This technique, which was previously used to create ceramic foams, presents additional difficulties when applied to titanium, due to its higher density, larger powder size and much higher reactivity with water. The main results are as follows.

- Using  $<45 \mu\text{m}$  Ti powders and ice front velocities of  $2\text{--}12 \mu\text{m s}^{-1}$ , foams were produced with 57–67% elongated pores, which were  $\sim 0.1 \text{ mm}$  in width and several millimeters in length. The pores were aligned along the freezing direction and their wall-to-wall distance varied with the local ice front velocity, in accordance with theoretical considerations.
- The as-received  $<45 \mu\text{m}$  Ti powders had very high oxygen content (3.4 wt.%), which increased by 0.4 wt.% during the freeze-casting procedure. As a result, the resulting freeze-cast foams showed high compressive strength (40–60 MPa for 60% porosity), but exhibited signs of embrittlement (stress serrations and crushing after 45% strain).
- While foams freeze-cast with coarser  $<125 \mu\text{m}$  powders contained only 0.24 wt.% O (well below the embrittling level), they exhibited lower porosities (39%) and these pores were not elongated. A simplified analysis correctly predicted that, for the present ice front velocities,  $<45 \mu\text{m}$  powders were rejected into interdendritic space so elongated pores could form, while  $<125 \mu\text{m}$  powder were engulfed by ice, thus preventing the formation of elongated pores.

#### Acknowledgements

This research was supported by US National Science Foundation through Grant DMR-0505772.

#### References

- [1] Queheillalt DT, Choi BW, Schwartz DS, Wadley HNG. Metall Mater Trans A 2000;31:261.
- [2] Dunand DC. Adv Eng Mater 2004;6:369.
- [3] Nilles JL, Karagian Mt, Wheeler KR. J Biomed Mater Res 1974;8:319.
- [4] Donachie M. Adv Mater Proc 1998;154:63.
- [5] Spoerke ED, Murray NG, Li H, Brinson LC, Dunand DC, Stupp SI. Acta Biomater 2005;1:523.
- [6] Ryan G, Pandit A, Apatsidis DP. Biomaterials 2006;27:2651.
- [7] Higuchi Y, Ohashi Y, Nakajima H. Adv Eng Mater 2006;8:907.
- [8] Wen CE, Yamada Y, Shimojima K, Chino Y, Asahina T, Mabuchi M. J Mater Sci Mater Med 2002;13:397.
- [9] Bram M, Stiller C, Buchkremer HP, Stover D, Baur H. Adv Eng Mater 2000;2:196.
- [10] Wen CE, Yamada Y, Shimojima K, Chino Y, Hosokawa H, Mabuchi M. J Mater Res 2002;17:2633.
- [11] Wen CE, Mabuchi M, Yamada Y, Shimojima K, Chino Y, Asahina T. Scripta Mater 2001;45:1147.

- [12] Kearns MW, Blenkinsop PA, Barber AC, Farthing TW. *Int J Powder Metall* 1988;24:59.
- [13] Davis NG, Teisen J, Schuh C, Dunand DC. *J Mater Res* 2001;16:1508.
- [14] Spoerke ED, Murray NGD, Li H, Brinson LC, Dunand DC, Stupp SI. *J Biomed Mater Res* 2007. doi:10.1002/jbm.a.31317.
- [15] Weiner S, Wagner HD. *Annu Rev Mater Sci* 1998;28:271.
- [16] Tuchinskiy L, Loutfy R. In: Shrivastava S, editor. *Materials and processes for medical devices*. Materials Park (OH): ASM International; 2003.
- [17] Mukai SR, Nishihara H, Tamon H. *Chem Commun* 2004:874.
- [18] Nishihara H, Mukai SR, Yamashita D, Tamon H. *Chem Mater* 2005;17:683.
- [19] Sofie SW, Dogan F. *J Am Ceram Soc* 2001;84:1459.
- [20] Araki K, Halloran JW. *J Am Ceram Soc* 2004;87:2014.
- [21] Araki K, Halloran JW. *J Am Ceram Soc* 2005;88:1108.
- [22] Deville S, Saiz E, Nalla RK, Tomsia AP. *Science* 2006;311:515.
- [23] Deville S, Saiz E, Tomsia AP. *Acta Mater* 2007;55:1965.
- [24] Jaffee RI, Ogden HR, Maykuth DJ. *AIME Trans* 1950;188:1261.
- [25] Miyawaki O, Yano T. *Jpn J Freez Dry* 1985;31:24.
- [26] Miyawaki O, Abe T, Yano T. *Biosci Biotech Biochem* 1992;56:953.
- [27] Miyawaki O, Fujii T, Shimiya Y. *Food Sci Technol Res* 2004;10:437.
- [28] Casses P, Azouni-Aidi MA. *Adv Colloid Interface Sci* 1994;50:103.
- [29] Larson I. *J Am Chem Soc* 1993;115:11885.
- [30] Watanabe T, Horikoshi Y. *Int J Powder Metall Powder Technol* 1976;12:209.
- [31] In: Lide DR, editor in-chief., 74th. ed. Boca Raton, FL: CRC Press Inc; 1993.
- [32] Azouni-Aidi MA, Casses P. *Adv Colloid Interface Sci* 1998;75:83.
- [33] Pourbaix M. *Atlas of electrochemical equilibria in aqueous solutions*. 2nd ed. Houston, TX: National Association of Corrosion Engineers; 1974.
- [34] Donachie Jr MJ. *Titanium – a technical guide*. 2nd ed. Materials Park OH: ASM International; 2000.
- [35] Frost HJ, Ashby MF. *Deformation-mechanism maps*. 1st ed. Oxford: Pergamon Press; 1982.
- [36] Takahashi Y, Nakamura T, Nishiguchi K. *J Mater Sci* 1992;27:485.
- [37] Gibson LJ, Ashby MF. *Cellular solids structure and properties*. 2nd ed. Cambridge, MA: Cambridge University Press; 1997.
- [38] Yamada Y, Shimojima K, Mabuchi M, Nakamura M, Asahina T, Mukai T, et al. *Mater Sci Eng A* 2000;277:213.